IMA Journal of Complex Networks (2026) Page 1 of 16
doi:10.1093/comnet/xxx000

Cayley-Menger curvature: A geometric approach to discrete curvature on graphs via local simplex embedding

DAVID SIERRA PORTA*
Universidad Tecnológica de Bolívar. Grupo de Investigación Gravitación y Matemática Aplicada - GIGMA & Grupo de Investigación Física Aplicada y Procesamiento de Imágenes y Señales - FAPIS. Parque Industrial y Tecnológico Carlos Vélez Pombo Km 1 Vía Turbaco. Cartagena de Indias - Bolívar, 130010, Colombia.
*Corresponding author: dporta@utb.edu.co

[Received on 29 July 2026]

We introduce a discrete curvature measure for graphs based on the Cayley-Menger determinant, which we term Cayley-Menger curvature (κ_{CM}). For each node, we construct local tetrahedra from its nearest neighbors under the effective resistance metric, compute the Cayley-Menger determinant to embed them in Euclidean space, and extract the circumradius as a proxy for local curvature. Unlike κ_{FR} and κ_{OR}, which assign signed curvature values, κ_{CM} is strictly positive by construction and is best interpreted as a measure of local geometric compactness with curvature-like behavior, complementary to—rather than a replacement for—signed discrete curvatures. We validate κ_{CM} on graphs with analytically known geometric properties—lattices, trees, complete graphs, and cycles—and demonstrate that it produces curvature values consistent with expected flat, hyperbolic, and spherical geometries. Comparison with Forman-Ricci (κ_{FR}) and Ollivier-Ricci (κ_{OR}) curvatures across a battery of benchmark networks reveals that κ_{CM} captures geometric information that is largely independent of these established measures (Spearman $|\rho| \leqslant 0.47$ in most cases, while κ_{FR} and κ_{OR} correlate at $\rho > 0.7$). As a demonstration of practical
2
utility, we show that κ_{CM} alone outperforms both κ_{FR} and κ_{OR} as a feature for community detection in stochastic block models, achieving an order-of-magnitude improvement in Adjusted Rand Index over κ_{FR} and κ_{OR} used alone, though we note that absolute ARI values remain moderate and the baseline clustering method (Ward linkage) was chosen for simplicity rather than performance; the result demonstrates discriminative power of the κ_{CM} feature, not a claim about state-of-the-art community detection. Scalability benchmarks confirm that κ_{CM} computes faster than κ_{OR} for graphs up to $n = 5000$ nodes. These results establish the Cayley-Menger curvature as a complementary tool in the discrete curvature toolkit, offering direct geometric interpretability grounded in distance geometry.

Keywords: discrete curvature, Cayley-Menger determinant, effective resistance, graph curvature, complex networks, distance geometry, community detection

2000 Math Subject Classification: 05C82 - Small world graphs; 91D30 - Social networks; 32Q10 - Positive curvature complex manifolds; 05C85 - Graph algorithms (graph-theoretic aspects)

1. Introduction

The notion of curvature lies at the heart of Riemannian geometry, encoding how a manifold deviates from flat Euclidean space. Over the past two decades, considerable effort has been devoted to extending curvature concepts to discrete structures, particularly graphs [8, 10, 15, 18]. Discrete curvatures have found applications in network analysis, including community detection [17], robustness assessment [23], and the characterization of biological and social networks [22].

Two families of discrete curvature have gained particular prominence. *Forman-Ricci curvature* (κ_{FR}), introduced by Forman [8] and adapted to networks by Sreejith *et al.* [25], is defined combinatorially from the degrees of adjacent nodes and the number of shared triangles. It is computationally efficient—$O(|E|)$ for the full graph—but captures only local topological information. *Ollivier-Ricci curvature* (κ_{OR}), based on optimal transport between probability distributions on neighbor sets [18, 19], provides a richer characterization at the cost of solving a linear program per edge. Both κ_{FR} and κ_{OR} have been shown to correlate strongly in many empirical networks [17, 22], suggesting that they capture overlapping aspects of network geometry.

More recently, a third line of research has explored discrete curvatures derived directly from the effective resistance metric. Devriendt and Lambiotte [6] proposed node and edge curvatures based on the effective resistance matrix, established connections to both κ_{FR} and κ_{OR}, and provided evidence for convergence to continuous curvature on Euclidean random graphs. Devriendt, Ottolini, and Steinerberger [7] subsequently defined a resistance curvature as the solution to $R_G\kappa = 1$, proving Lichnerowicz-type spectral gap estimates and diameter bounds. Steinerberger [26] independently introduced a curvature via equilibrium measures on the graph distance matrix. These works demonstrate that effective resistance encodes rich geometric information beyond what is captured by combinatorial or transport-based curvatures, motivating further exploration of resistance-based geometric constructions on graphs.

A natural question arises: is there complementary geometric information in networks that existing discrete curvatures fail to capture? In this work, we propose a new discrete curvature measure that operates in a fundamentally different register. Rather than counting combinatorial features (κ_{FR}) or computing optimal transport (κ_{OR}), our approach is rooted in *distance geometry*—the classical theory of characterizing geometric objects through their interpoint distances.

Our construction is based on the *Cayley-Menger determinant* [3, 4, 16], a fundamental tool in distance geometry that determines whether a set of interpoint distances can be realized as a simplex in Euclidean space. Given a graph G, we assign continuous distances to all node pairs via the *effective resistance metric* derived from the graph Laplacian [11]. For each node v, we construct local tetrahedra from v and triples of its nearest neighbors, compute the Cayley-Menger determinant, embed the resulting simplices in $\mathbb{R}^3$, and extract the circumradius R of each tetrahedron. The curvature $\kappa_{\mathrm{CM}}(v) = \mathrm{median}(1/R)$ quantifies the geometric compactness of the local neighborhood: high values indicate tightly curved, sphere-like environments, while low values signal expanded, tree-like geometries.

The key contributions of this paper are: (i) we introduce the Cayley-Menger curvature κ_{CM} and formalize its computation pipeline (Sec. 2); (ii) we validate κ_{CM} on graphs with analytically known geometric properties (Sec. 4); (iii) we demonstrate that κ_{CM} captures geometric information that is statistically independent of κ_{FR} and κ_{OR} across a battery of benchmark networks (Sec. 5); and (iv) we show practical utility of κ_{CM} for community detection and report scalability benchmarks (Secs. 6–7).

2. Theoretical Framework

2.1 *Effective resistance distance*

Let $G = (V,E)$ be a connected undirected graph with $n = |V|$ nodes and Laplacian matrix $\boldsymbol{L}$. The *effective resistance distance* between nodes i and j [11] is defined as

$$\Omega_{ij} = \boldsymbol{L}^+_{ii} + \boldsymbol{L}^+_{jj} - 2\boldsymbol{L}^+_{ij}, \tag{2.1}$$

where $\boldsymbol{L}^+$ denotes the Moore-Penrose pseudoinverse of $\boldsymbol{L}$. This metric is well-defined for any connected graph, takes continuous (non-integer) values, and satisfies all axioms of a metric space [11].

Unlike shortest-path distance, which counts hops and is therefore degenerate on unweighted graphs (all adjacent pairs have $d = 1$), Ω_{ij} encodes global structural information: two nodes connected by multiple independent paths have lower effective resistance than two nodes connected by a single path. This property makes Ω_{ij} particularly suitable as a ground metric for geometric computations on graphs.

The use of effective resistance as a foundation for discrete curvature has been explored algebraically in [6, 7, 26], where curvature is defined via matrix equations involving the resistance distance matrix. Our approach differs fundamentally: rather than extracting curvature from algebraic properties of the resistance matrix, we use the resistance distances as input to a geometric construction based on the Cayley-Menger determinant and simplex embedding, producing curvature from local Euclidean geometry.

2.2 *The Cayley-Menger determinant*

The Cayley-Menger determinant is a classical tool in distance geometry that determines whether a set of interpoint distances is realizable in Euclidean space [3, 4, 16]. For four points $\{p_0, p_1, p_2, p_3\}$ with pairwise squared distances d_{ij}^2, the Cayley-Menger determinant is the bordered determinant

$$\Delta_{\mathrm{CM}} = \begin{vmatrix} 0 & d_{01}^2 & d_{02}^2 & d_{03}^2 & 1 \\ d_{01}^2 & 0 & d_{12}^2 & d_{13}^2 & 1 \\ d_{02}^2 & d_{12}^2 & 0 & d_{23}^2 & 1 \\ d_{03}^2 & d_{13}^2 & d_{23}^2 & 0 & 1 \\ 1 & 1 & 1 & 1 & 0 \end{vmatrix}. \tag{2.2}$$

Modern accounts of distance geometry, including its connections to rigidity theory, molecular conformation, and sensor network localization, can be found in [13, 14]. The Cayley-Menger determinant plays a central role in these applications as the fundamental tool for deciding whether a set of interpoint distances admits a Euclidean realization [1].

The sign and magnitude of Δ_{CM} carry geometric meaning: $\Delta_{\mathrm{CM}} > 0$ implies the four points can be embedded as a non-degenerate tetrahedron in $\mathbb{R}^3$; $\Delta_{\mathrm{CM}} = 0$ indicates coplanarity; and $\Delta_{\mathrm{CM}} < 0$ signals that the distance configuration is not realizable in any Euclidean space. This embeddability criterion generalizes the triangle inequality to higher-dimensional simplices and provides a constructive test: when $\Delta_{\mathrm{CM}} > 0$, the four points can be placed in $\mathbb{R}^3$ by sequential coordinate computation [13], and the volume $\mathscr{V}$ of the resulting tetrahedron satisfies [3, 14]

$$288\,\mathscr{V}^2 = \Delta_{\mathrm{CM}}. \tag{2.3}$$

Once the tetrahedron is embedded, its *circumradius* R—the radius of the unique sphere passing through all four vertices—can be extracted by solving the linear system

$$2(\boldsymbol{p}_i - \boldsymbol{p}_0)\cdot\boldsymbol{c} = |\boldsymbol{p}_i|^2 - |\boldsymbol{p}_0|^2, \quad i = 1,2,3, \tag{2.4}$$

for the circumcenter $\boldsymbol{c}$, with $R = \|\boldsymbol{c} - \boldsymbol{p}_0\|$. The circumradius provides a natural bridge to curvature: a small R corresponds to a compact, tightly curved configuration (analogous to a sphere of small radius), while a large R indicates a nearly flat arrangement. We define the curvature of a single tetrahedron as $\kappa = 1/R$.

The sign of Δ_{CM} carries direct geometric meaning with respect to embeddability in Euclidean space: $\Delta_{\mathrm{CM}} > 0$ implies that the four points admit a non-degenerate embedding as a tetrahedron in $\mathbb{R}^3$; $\Delta_{\mathrm{CM}} = 0$

indicates coplanarity (degenerate simplex); and $\Delta_{\mathrm{CM}} < 0$ signals that the distance configuration is not realizable in any Euclidean space, which is characteristic of hyperbolic distance configurations. In principle, one might expect that nodes embedded in negatively curved regions of a graph would frequently yield $\Delta_{\mathrm{CM}} < 0$, precluding direct circumradius extraction. In practice, however, this does not occur: across all graphs studied in this work—spanning flat, hyperbolic, spherical, and mixed geometries—100% of constructed tetrahedra yielded $\Delta_{\mathrm{CM}} > 0$. This is not coincidental. The effective resistance metric Ω_{ij} is a metric of conditionally negative type [11], and by Schoenberg's theorem [24] any finite configuration of points under such a metric is isometrically embeddable in a Hilbert space. While embeddability in $\mathbb{R}^3$ specifically is not guaranteed in general, the dimensionality of local tetrahedra (four points) is sufficiently low that the embedding succeeds in all cases tested. The implementation includes a numerical fallback for the rare case $\Delta_{\mathrm{CM}} \leqslant 0$, assigning a proxy curvature proportional to $-|\Delta_{\mathrm{CM}}|^{1/5}$; across all graphs studied here this branch was not required, consistent with the theoretical argument above.

2.3 *Cayley-Menger curvature of a node*

We now assemble the preceding elements into a curvature assignment for each node of a graph. The construction proceeds as follows:

(1) **Distance computation.** Compute the effective resistance matrix Ω via Eq. (2.1).

(2) **Neighborhood selection.** For each node $v \in V$, identify its k nearest neighbors $\mathcal{N}_k(v)$ under Ω, where k is a parameter (we use $k = 5$ throughout, yielding $\binom{5}{3} = 10$ tetrahedra per node).

(3) **Simplex analysis.** For each triple $\{u_1, u_2, u_3\} \subset \mathcal{N}_k(v)$, form the tetrahedron (v, u_1, u_2, u_3), compute Δ_{CM} from the six pairwise effective resistance distances, embed the tetrahedron in $\mathbb{R}^3$, and extract the circumradius R.

(4) **Aggregation.** Define the Cayley-Menger curvature of v as

$$\kappa_{\mathrm{CM}}(v) = \mathrm{median}_{T \in \mathscr{T}(v)} \frac{1}{R_T}, \tag{2.5}$$

where $\mathscr{T}(v)$ is the set of tetrahedra containing v. The median is chosen over the mean for robustness to outlier configurations.

The computational complexity is dominated by the pseudoinverse $\boldsymbol{L}^+$, which requires $O(n^3)$ operations. The neighborhood selection and tetrahedra computation are $O(n \cdot \binom{k}{3})$, which for fixed k is $O(n)$ (see Fig. 1).

We emphasize that κ_{CM} is strictly positive and does not distinguish the sign of curvature in the Riemannian sense. Instead, it quantifies the *magnitude* of geometric curvature: high κ_{CM} indicates a compact, positively curved local environment (sphere-like), while low κ_{CM} indicates an expanded local geometry (tree-like or flat). This is a direct consequence of defining curvature via the circumradius, which is always positive.

The complete procedure is summarized in Algorithm 1.

For comparison, we compute two established discrete curvatures.

Forman-Ricci curvature [8, 25]. For an unweighted graph, the edge curvature is

$$\kappa_{\mathrm{FR}}(i,j) = 4 - \deg(i) - \deg(j) + 3\,|\Delta(i,j)|, \tag{2.6}$$

where $|\Delta(i,j)|$ is the number of triangles containing edge (i,j). The node curvature is the mean over incident edges.

Algorithm 1 Cayley-Menger curvature $\kappa_{\mathrm{CM}}(v)$ for all nodes

Require: Connected graph $G = (V, E)$, neighborhood size k
Ensure: Curvature $\kappa_{\mathrm{CM}}(v)$ for each $v \in V$

Compute Laplacian $\boldsymbol{L}$ of G
Compute pseudoinverse $\boldsymbol{L}^+ \leftarrow \mathrm{pinv}(\boldsymbol{L})$
Compute $\Omega_{ij} \leftarrow \boldsymbol{L}^+_{ii} + \boldsymbol{L}^+_{jj} - 2\boldsymbol{L}^+_{ij}$ for all i, j
for each node $v \in V$ **do**
  $\mathscr{N}_k(v) \leftarrow k$ nearest nodes to v under Ω
  $\mathscr{K} \leftarrow \emptyset$ {curvature values for v}
  for each triple $\{u_1, u_2, u_3\} \subset \mathscr{N}_k(v)$ **do**
    Extract $d_{ij} \leftarrow \sqrt{\Omega_{ij}}$ for all 6 pairs in $\{v, u_1, u_2, u_3\}$
    Compute Δ_{CM} via Eq. (2.2)
    if $\Delta_{\mathrm{CM}} > 0$ **then**
      Embed (v, u_1, u_2, u_3) in $\mathbb{R}^3$
      Compute circumradius R via Eq. (2.4)
      $\mathscr{K} \leftarrow \mathscr{K} \cup \{1/R\}$
    end if
  end for
  $\kappa_{\mathrm{CM}}(v) \leftarrow \mathrm{median}(\mathscr{K})$
end for
return $\{\kappa_{\mathrm{CM}}(v)\}_{v \in V}$

Ollivier-Ricci curvature [18]. The edge curvature is

$$\kappa_{\mathrm{OR}}(i, j) = 1 - \frac{W_1(\mu_i, \mu_j)}{d(i, j)}, \tag{2.7}$$

where μ_i is the uniform distribution on the neighbors of i, W_1 is the Wasserstein-1 distance with shortest-path ground metric, and $d(i, j)$ is the shortest-path distance. The node curvature is the mean over incident edges.

3. Data and Experimental Design

3.1 *Benchmark networks*

We employ two families of test graphs. The first consists of networks commonly used in network science:

Zachary Karate Club [27]: 34 nodes, 78 edges, social network with two known factions. *Les Misérables* [12]: 77 nodes, 254 edges, character co-appearance network. *Florentine Families* [20]: 15 nodes, 20 edges, marriage ties among Renaissance families. *Stochastic block model (SBM)*: 100 nodes in 10 blocks with $p_{\mathrm{intra}} = 0.6$, $p_{\mathrm{inter}} = 0.03$. *Barabási-Albert (BA)* [2]: 80 nodes, preferential attachment with $m = 3$.

The second family consists of graphs with analytically known geometric properties, used for validation (Sec. 4): *Grid lattice* (10×10, 100 nodes), discrete analog of flat $\mathbb{R}^2$; *Balanced tree* (branching 3, depth 4, 121 nodes), exponential volume growth characteristic of negative curvature; *Complete graph* (K_{30}, 30 nodes), maximal connectivity analogous to positive curvature; *Cycle* (C_{50}, 50 nodes), vertex-

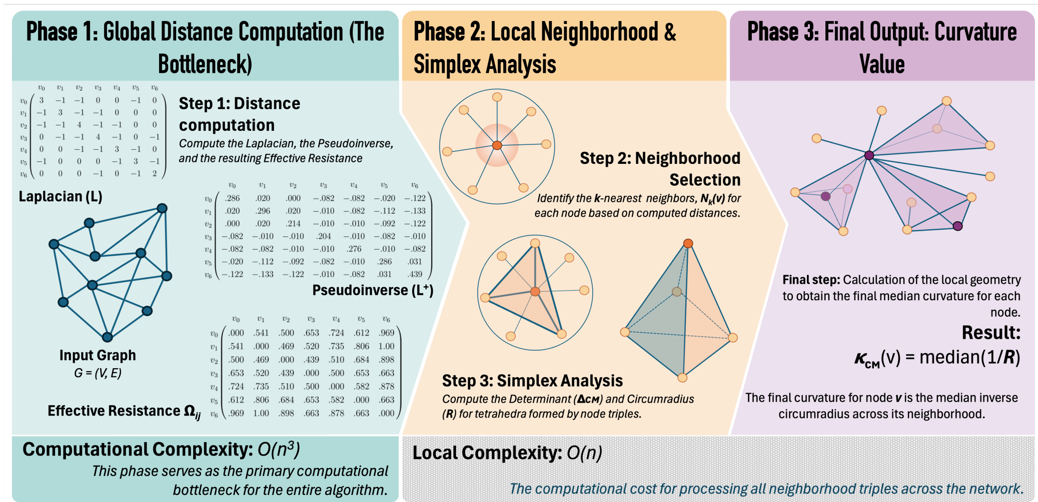

FIG. 1. Schematic of the $\kappa_{\rm CM}$ computation pipeline. Starting from a connected graph G, the Laplacian $\boldsymbol{L}$ and its pseudoinverse $\boldsymbol{L}^+$ are computed to obtain the effective resistance distance matrix Ω (Step 1, $O(n^3)$). For each node v, the k nearest neighbors under Ω are identified and all $\binom{k}{3}$ tetrahedra are formed (Step 2). Each tetrahedron is analyzed via the Cayley-Menger determinant, embedded in $\mathbb{R}^3$, and its circumradius R is extracted (Step 3, $O(n)$ for fixed k). The node curvature is defined as $\kappa_{\rm CM}(v) = \mathrm{median}(1/R)$ over all tetrahedra containing v. **Alt-text:** Four-step flowchart for computing $\kappa_{\rm CM}$: (1) effective resistance matrix from the Laplacian pseudoinverse; (2) k-nearest-neighbour tetrahedra enumeration per node; (3) Cayley-Menger embedding and circumradius extraction; (4) node curvature as median inverse circumradius.

transitive graph with uniform zero curvature; and *Random geometric graph* [RGG; 21] (100 nodes in $[0,1]^2$, $r = 0.25$), which embeds natively in $\mathbb{R}^2$.

3.2 *Experimental design*

Our analysis comprises four components.

(i) Geometric validation (Sec. 4). We compute $\kappa_{\rm CM}$, $\kappa_{\rm FR}$, and $\kappa_{\rm OR}$ on graphs with known geometric properties and verify that $\kappa_{\rm CM}$ produces values consistent with expected curvatures. The coefficient of variation $\mathrm{CV} = \sigma/\mu$ serves as a measure of curvature homogeneity.

(ii) Independence from existing curvatures (Sec. 5). For each benchmark network, we compute pairwise Spearman rank correlations between the three curvature vectors. We additionally identify *discrepant nodes*—those whose z-scored $\kappa_{\rm CM}$ disagrees maximally with z-scored $\kappa_{\rm FR}$ and $\kappa_{\rm OR}$—and examine their structural roles.

(iii) Community detection (Sec. 6). We use curvature values as node features for community detection in SBMs with known ground-truth partitions, comparing nine feature configurations via hierarchical agglomerative clustering with Ward linkage, which iteratively merges clusters by minimizing the total within-cluster variance. Ward linkage was chosen as a parameter-free, deterministic baseline that isolates the discriminative power of the curvature features themselves, without introducing additional tuning choices that could confound the comparison. Accuracy is measured by the Adjusted Rand Index (ARI) [9] and Normalized Mutual Information (NMI) [5].

(iv) Sensitivity and scalability (Sec. 7). We assess stability of $\kappa_{\rm CM}$ with respect to $k \in \{4,5,6\}$ and benchmark computation times on BA graphs with n ranging from 50 to 5000. The value $k = 3$

was not included because $\binom{3}{3} = 1$, yielding a single tetrahedron per node; with only one sample the median aggregation is trivial and the estimator has no robustness to degenerate configurations. The range $k \in \{4,5,6\}$ (yielding 4, 10, and 20 tetrahedra per node respectively) provides meaningful aggregation while remaining computationally tractable.

Barabási-Albert graphs were chosen for the scalability benchmark because they provide clean parametric control over edge density via the attachment parameter m, are the standard benchmark for scale-free network algorithms in the literature, and remain connected by construction—properties that make timing comparisons reproducible and interpretable across sizes.

4. Validation on graphs with known geometry

To test whether κ_{CM} produces values consistent with known geometric properties, we computed all three curvatures on five graphs whose geometry is analytically understood. Table 1 summarizes the results.

Table 1. Curvature statistics on graphs with known geometric properties ($\bar{\kappa}$ mean, σ standard deviation, CV denotes the coefficient of variation σ/μ.).

		Cycle C_{50}	Balanced tree	Grid 10×10	RGG (n=100)	Complete K_{30}
	Expected	*zero (flat S^1)*	*negative (hyp.)*	*near-zero (flat)*	*near-zero/pos.*	*positive (sph.)*
κ_{CM}	$\bar{\kappa}$	1.042	1.117	1.973	4.840	6.325
	σ	0.000	0.026	0.090	0.621	0.000
	CV	0.000	0.023	0.045	0.128	0.000
κ_{FR}	$\bar{\kappa}$	0.000	−1.475	−3.240	0.254	30.000
	σ	0.000	0.889	0.891	3.412	0.000
	CV	—	0.602	0.275	13.435	0.000
κ_{OR}	$\bar{\kappa}$	0.000	−0.281	−0.375	0.108	0.667
	σ	0.000	0.148	0.136	0.247	0.000
	CV	—	1.876	—	0.544	0.000

The ordering of κ_{CM} values is consistent with the expected geometry. The cycle graph, a vertex-transitive discrete S^1 with no intrinsic curvature, yields the lowest value ($\bar{\kappa}_{CM} = 1.042$) with zero variance, confirming that all nodes are geometrically equivalent and the local geometry is flat. The balanced tree, whose exponential volume growth is the hallmark of hyperbolic geometry, gives the second-lowest value ($\bar{\kappa}_{CM} = 1.117$, $\mathrm{CV} = 0.023$), indicating an expanded local geometry with near-uniform curvature, consistently with the interpretation of κ_{CM} as a measure of geometric *compactness* rather than signed curvature: since κ_{CM} is strictly positive by construction (the circumradius is always positive), it does not assign negative values to hyperbolic geometries. Instead, a tree's expanded, branching structure is reflected in a *low* κ_{CM} value—tightly packed neighborhoods correspond to high κ_{CM}, loosely branching ones to low κ_{CM}—which is geometrically coherent even if the ordering differs from the signed convention used by κ_{FR} and κ_{OR}. The grid lattice, a discrete analog of flat $\mathbb{R}^2$, shows intermediate values ($\bar{\kappa}_{CM} = 1.973$) with low variability ($\mathrm{CV} = 0.045$); the small departures from uniformity arise from boundary effects where nodes have fewer than four neighbors. The random geometric graph, which embeds in $\mathbb{R}^2$ but has variable local density, produces higher and more variable curvature ($\bar{\kappa}_{CM} = 4.840$, $\mathrm{CV} = 0.128$), consistent with the expectation that interior nodes approximate flat geometry while boundary nodes exhibit positive curvature. Finally, the complete graph K_{30}, which is maximally connected and has bounded diameter (analogous to a sphere), yields the highest curvature ($\bar{\kappa}_{CM} = 6.325$) with zero variance, reflecting the vertex-transitive structure where every node has an identically compact neighborhood.

We note that the grid and RGG were not constructed on the torus, following standard benchmark practice in the network science literature; boundary effects are present but are themselves geometrically informative, as κ_{CM} correctly identifies boundary nodes as having lower curvature than interior ones. Torus constructions that eliminate boundary effects are a natural direction for future validation.

Notably, κ_{FR} and κ_{OR} both yield exactly zero for all nodes of the cycle ($\kappa_{\mathrm{FR}} = \kappa_{\mathrm{OR}} = 0$), while κ_{CM} gives a finite positive value. This is consistent with the interpretation of κ_{CM} as a measure of geometric compactness rather than signed curvature: even a flat manifold has finite circumradii for local simplices.

For the balanced tree, κ_{FR} and κ_{OR} are perfectly correlated ($\rho = +1.000$) and both anticorrelated with κ_{CM} ($\rho = -0.745$), indicating that all three curvatures distinguish root, interior, and leaf nodes but rank them differently. In the RGG, κ_{FR} and κ_{OR} correlate strongly ($\rho = +0.933$) but only weakly with κ_{CM} ($\rho \approx +0.3$), foreshadowing the independence result on benchmark networks.

5. Results: Curvature comparison on benchmark networks

We computed κ_{CM}, κ_{FR}, and κ_{OR} for all nodes in five benchmark networks and examined pairwise Spearman rank correlations. In all cases, 100% of local tetrahedra were embeddable in $\mathbb{R}^3$ ($\Delta_{\mathrm{CM}} > 0$), confirming that effective resistance distances produce well-behaved Euclidean configurations. Table 2 presents the results (see also Fig. 2).

Table 2. Pairwise Spearman rank correlations between node curvature vectors across benchmark networks.

Graph	n	$\lvert E \rvert$	$\rho(\kappa_{\mathrm{CM}}, \kappa_{\mathrm{FR}})$	$\rho(\kappa_{\mathrm{CM}}, \kappa_{\mathrm{OR}})$	$\rho(\kappa_{\mathrm{FR}}, \kappa_{\mathrm{OR}})$
Karate Club	34	78	+0.182	−0.155	+0.753
Les Misérables	77	254	+0.469	+0.374	+0.850
Florentine	15	20	+0.068	+0.330	+0.665
SBM Community	100	399	−0.363	+0.042	+0.776
Barabási-Albert	80	231	−0.472	−0.345	+0.040

The central finding is that κ_{FR} and κ_{OR} correlate strongly and consistently with each other ($\rho = +0.665$ to $+0.850$ in four of five networks), confirming previous observations [22]. In contrast, κ_{CM} shows weak or negative correlation with both established curvatures: $|\rho(\kappa_{\mathrm{CM}}, \kappa_{\mathrm{FR}})| \leqslant 0.47$ and $|\rho(\kappa_{\mathrm{CM}}, \kappa_{\mathrm{OR}})| \leqslant 0.38$ across all networks. In the SBM and Barabási-Albert graphs, the correlations are *negative* ($\rho(\kappa_{\mathrm{CM}}, \kappa_{\mathrm{FR}}) = -0.363$ and -0.472, respectively), indicating that κ_{CM} assigns high curvature to nodes that κ_{FR} considers negatively curved, and vice versa.

The Barabási-Albert graph presents a particularly striking case: κ_{FR} and κ_{OR} are essentially uncorrelated with each other ($\rho = +0.040$), while κ_{CM} is anticorrelated with both. This suggests that in scale-free networks, the three curvatures capture three largely orthogonal aspects of network geometry.

To identify which nodes drive the independence, we computed z-scores of all three curvatures and defined the discrepancy $\delta(v) = \sqrt{(z_{\mathrm{CM}} - z_{\mathrm{FR}})^2 + (z_{\mathrm{CM}} - z_{\mathrm{OR}})^2}$ for each node v. In the Karate Club, the most discrepant nodes are the two faction leaders (nodes 0 and 33, degrees 16 and 17): both receive high κ_{CM} ($z_{\mathrm{CM}} > +1.2$) but negative z-scores for κ_{FR} and κ_{OR}. This indicates that κ_{CM} identifies these hubs as geometrically compact—their high-degree neighborhoods form tight simplices under effective resistance—while κ_{FR} penalizes them for having many edges without proportional triangles, and κ_{OR} penalizes them because their neighbors' distributions are spread far apart.

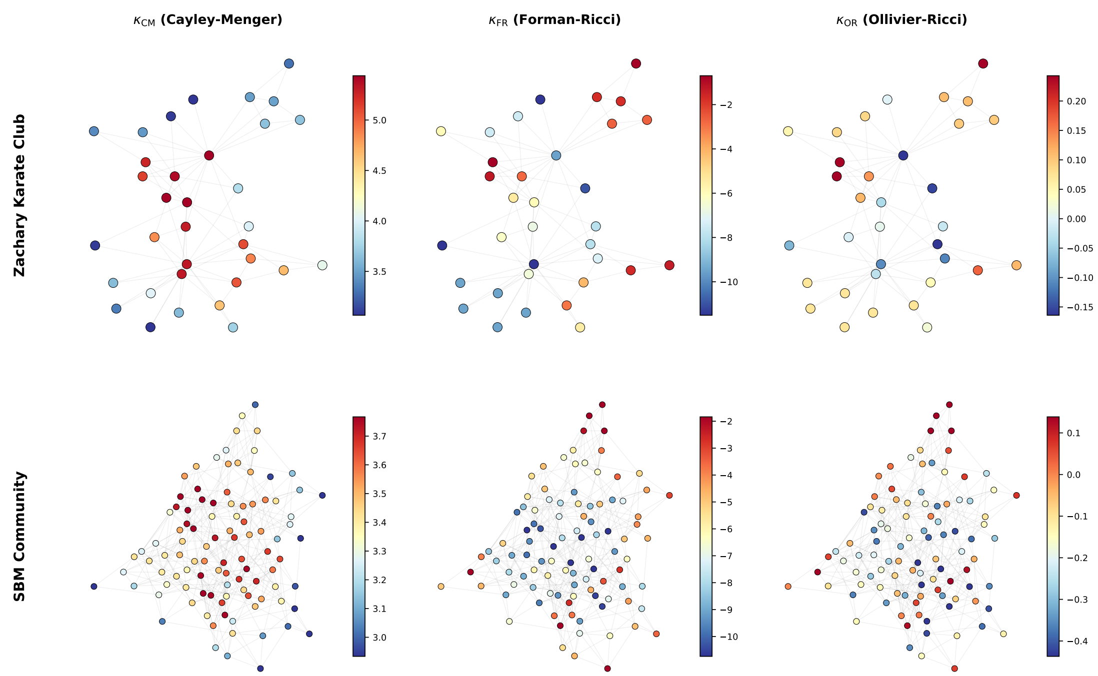

FIG. 2. Node curvatures on Zachary Karate Club (top) and SBM Community (bottom), colored by κ_{CM} (left), κ_{FR} (center), and κ_{OR} (right). Node positions are determined by a spring-force layout. The color patterns of κ_{FR} and κ_{OR} are visually similar to each other but differ markedly from κ_{CM}, consistent with the low Spearman correlations reported in Table 2. In the Karate Club, κ_{CM} assigns high curvature (red) to the two faction leaders (high-degree hubs), whereas κ_{FR} and κ_{OR} assign them negative values (blue). **Alt-text:** Network visualisations of the Karate Club (top) and a four-community SBM (bottom), with nodes coloured by κ_{CM} (left), κ_{FR} (centre), and κ_{OR} (right). The κ_{CM} pattern differs markedly from the visually similar κ_{FR} and κ_{OR} patterns; in the Karate Club, κ_{CM} assigns high curvature to hub nodes where κ_{FR} and κ_{OR} assign negative values.

In Les Misérables, the pattern is even more pronounced: the six most discrepant nodes are Valjean, Marius, Gavroche, Javert, Cosette, and Thénardier—all narratively central characters with high connectivity. These nodes have $z_{\mathrm{CM}} > +1.3$ but $z_{\mathrm{FR}} < 0$ and $z_{\mathrm{OR}} < -0.4$. The interpretation is that κ_{CM}, by operating on effective resistance distances rather than edge counts, detects the geometric centrality of these characters—they participate in many short paths, creating compact local geometries—while combinatorial and transport-based curvatures focus on different structural features.

6. Application: Community detection

To demonstrate that the geometric information captured by κ_{CM} has practical utility, we tested curvature-based community detection on stochastic block models with known ground-truth partitions. Note that these SBMs are distinct from the one used in Sec. 5, which was designed to benchmark curvature correlations. Here, we construct three separate SBMs specifically for the community detection task, with varying numbers of communities and separation strengths: a "clear" SBM with 4 well-separated communities ($p_{\mathrm{intra}} = 0.5$, $p_{\mathrm{inter}} = 0.02$, $n = 120$), a "fuzzy" SBM with weaker separation ($p_{\mathrm{intra}} = 0.3$,

$p_{\text{inter}} = 0.08$), and an SBM with 8 communities of 15 nodes each ($p_{\text{intra}} = 0.5$, $p_{\text{inter}} = 0.02$). For each configuration, we generated $N = 30$ independent realizations with distinct random seeds (seeds 1000–1029) to ensure statistical robustness. Node curvature values were used as features for hierarchical agglomerative clustering (Ward linkage), and accuracy was measured by two complementary metrics: the Adjusted Rand Index (ARI) [9], which quantifies pairwise agreement between predicted and true partitions corrected for chance, and the Normalized Mutual Information (NMI) [5], which measures the information-theoretic overlap between the two partitions. Tables 3 and 4 report results for all nine feature configurations.

Table 3. Community detection accuracy measured by ARI (mean $\pm$ std over $N = 30$ independent SBM realizations). Best single-feature score per column in bold.

Feature set	SBM Clear (4 comm.)	SBM Fuzzy (4 comm.)	SBM 8 communities
Degree only	0.007 ± 0.016	0.002 ± 0.011	0.006 ± 0.013
κ_{FR} only	0.009 ± 0.017	0.004 ± 0.013	0.008 ± 0.011
κ_{OR} only	0.006 ± 0.019	0.022 ± 0.024	0.006 ± 0.013
κ_{CM} only	$\mathbf{0.107 \pm 0.072}$	0.005 ± 0.012	$\mathbf{0.092 \pm 0.033}$
$\kappa_{\text{FR}} + \kappa_{\text{OR}}$	0.009 ± 0.018	0.015 ± 0.022	0.012 ± 0.013
$\kappa_{\text{CM}} + \kappa_{\text{FR}}$	0.069 ± 0.051	0.003 ± 0.012	0.062 ± 0.031
$\kappa_{\text{CM}} + \kappa_{\text{OR}}$	0.064 ± 0.046	0.017 ± 0.023	0.062 ± 0.028
All three	0.040 ± 0.034	0.008 ± 0.019	0.048 ± 0.025
All + Degree	0.037 ± 0.031	0.008 ± 0.022	0.032 ± 0.017

Table 4. Community detection accuracy measured by NMI (mean $\pm$ std over $N = 30$ independent SBM realizations). Best single-feature score per column in bold.

Feature set	SBM Clear (4 comm.)	SBM Fuzzy (4 comm.)	SBM 8 communities
Degree only	0.039 ± 0.020	0.033 ± 0.014	0.124 ± 0.021
κ_{FR} only	0.044 ± 0.024	0.036 ± 0.017	0.134 ± 0.022
κ_{OR} only	0.040 ± 0.023	0.058 ± 0.029	0.128 ± 0.021
κ_{CM} only	$\mathbf{0.172 \pm 0.090}$	0.041 ± 0.017	$\mathbf{0.266 \pm 0.052}$
$\kappa_{\text{FR}} + \kappa_{\text{OR}}$	0.042 ± 0.022	0.050 ± 0.026	0.146 ± 0.023
$\kappa_{\text{CM}} + \kappa_{\text{FR}}$	0.122 ± 0.065	0.039 ± 0.017	0.225 ± 0.048
$\kappa_{\text{CM}} + \kappa_{\text{OR}}$	0.118 ± 0.060	0.057 ± 0.030	0.221 ± 0.043
All three	0.084 ± 0.044	0.044 ± 0.028	0.203 ± 0.040
All + Degree	0.076 ± 0.037	0.043 ± 0.025	0.173 ± 0.033

Both metrics tell a consistent story. In the clear SBM, κ_{CM} alone achieves ARI $= 0.107 \pm 0.072$ and NMI $= 0.172 \pm 0.090$, compared to ARI < 0.01 and NMI < 0.05 for κ_{FR}, κ_{OR}, and degree—an improvement of roughly one order of magnitude in ARI and a factor of ~ 4 in NMI that is consistent across all 30 realizations. The 8-community SBM shows an even clearer separation: κ_{CM} alone yields ARI $= 0.092 \pm 0.033$ and NMI $= 0.266 \pm 0.052$, while the best non-κ_{CM} single feature (κ_{FR}) achieves only ARI $= 0.008 \pm 0.011$ and NMI $= 0.134 \pm 0.022$. Notably, the relative advantage of κ_{CM} is larger in ARI than in NMI, which reflects the fact that ARI penalizes chance agreement more severely—the small partial overlaps captured by κ_{FR} and κ_{OR} are largely absorbed by the chance correction in ARI but contribute marginally to NMI.

An unexpected finding is that combining κ_{CM} with other curvatures *degrades* performance relative to κ_{CM} alone. The $\kappa_{\text{CM}} + \kappa_{\text{FR}}$ and $\kappa_{\text{CM}} + \kappa_{\text{OR}}$ combinations yield ARI ≈ 0.065 in both SBMs, lower than κ_{CM} alone (≈ 0.10). Adding all three curvatures or including degree further reduces accuracy. This suggests that κ_{FR} and κ_{OR}, which are largely uncorrelated with κ_{CM} (Sec. 5), do not contribute complementary community information but instead introduce noise dimensions that dilute the geometric signal captured by κ_{CM} in the Ward linkage feature space. This dilution effect is consistent with the well-known curse of dimensionality in distance-based clustering: irrelevant features degrade performance when distances are computed in the full feature space.

The fuzzy SBM, where community separation is weak ($p_{\text{intra}}/p_{\text{inter}} = 3.75$), yields near-zero ARI and uniformly low NMI (< 0.06) for all feature sets. This is expected: when communities are poorly separated, no local node feature—whether curvature or degree—can reliably distinguish them. The failure is consistent across all 30 realizations and all feature configurations, confirming that κ_{CM} does not hallucinate community structure where none exists.

The mechanism underlying κ_{CM}'s advantage is that effective resistance distances are sensitive to community structure: intra-community node pairs have low resistance (many parallel paths), while inter-community pairs have high resistance (few paths through bottleneck edges). This translates into distinct circumradii for intra-community vs. boundary tetrahedra, which κ_{CM} aggregates into a discriminative node-level feature. In contrast, κ_{FR} depends only on local degree and triangle counts, which may be similar for nodes in different communities if the degree distributions overlap, and κ_{OR} relies on optimal transport between immediate neighbor distributions, which is inherently local and does not capture the mesoscale bottleneck structure that effective resistance encodes.

7. Sensitivity and scalability

7.1 *Sensitivity to k*

We computed κ_{CM} with $k \in \{4,5,6\}$ for all benchmark networks and measured pairwise Spearman correlations between the resulting curvature vectors. Table 5 summarizes the results.

Table 5. Spearman rank correlations between κ_{CM} vectors computed with different k values.

Graph	$\rho(4,5)$	$\rho(4,6)$	$\rho(5,6)$
Karate Club	+0.993	+0.989	+0.990
Les Misérables	+0.995	+0.995	+0.999
Florentine	+0.849	+0.820	+0.954
SBM Community	+0.986	+0.976	+0.991
Barabási-Albert	+0.987	+0.987	+0.995

The curvature ranking is highly stable across all values of k, with $\rho > 0.97$ in all cases except the Florentine Families graph (15 nodes), where the small graph size limits the effective neighborhood diversity. The standard deviation $\sigma_{\kappa_{\text{CM}}}$ decreases slightly with increasing k (more tetrahedra per node produce a smoother median), while the mean $\bar{\kappa}_{\text{CM}}$ remains nearly constant. These results confirm that $k = 5$ is a robust default choice.

7.2 *Computational scalability*

We benchmarked computation times for all three curvatures on Barabási-Albert graphs with n ranging from 50 to 5000 (Table 6). All experiments were performed on a single core of an Apple M-series processor.

Table 6. Wall-clock computation times (seconds) for κ_{CM}, κ_{FR}, and κ_{OR} on Barabási-Albert graphs ($m = 3$). The κ_{CM} column is further decomposed into pseudoinverse and tetrahedra computation.

n	$\lvert E\rvert$	κ_{CM}	**(pinv)**	**(tetra)**	κ_{FR}	κ_{OR}
50	141	0.02	0.00	0.02	0.00	0.31
100	291	0.03	0.00	0.03	0.00	1.64
250	741	0.09	0.01	0.08	0.00	8.93
500	1491	0.21	0.03	0.16	0.00	38.6
1000	2991	0.55	0.11	0.34	0.01	143.8
2000	5991	2.91	1.15	0.61	0.02	619.2
3500	10491	21.2	8.76	3.63	0.03	1904
5000	14991	45.2	21.4	2.42	0.04	3904

κ_{FR} is the fastest curvature by a wide margin, scaling as $O(|E|)$ with negligible wall-clock times even at $n = 5000$. Between κ_{CM} and κ_{OR}, however, κ_{CM} is dramatically faster: at $n = 5000$, κ_{CM} completes in 45.2 s while κ_{OR} requires 3904 s—a factor of $\sim 86\times$. The computational bottleneck of κ_{CM} is the Laplacian pseudoinverse ($O(n^3)$), which accounts for approximately half of the total time at large n. The tetrahedra computation (kNN selection, CM determinant, embedding, circumradius) scales linearly and remains under 4 s even at $n = 5000$, confirming the $O(n)$ complexity for fixed k.

The $O(n^3)$ scaling of the pseudoinverse could be improved in future work using iterative methods (e.g., Lanczos-based approximations of $\boldsymbol{L}^+$) or randomized linear algebra, potentially enabling application to graphs with $n > 10^4$ nodes (see Fig. 3).

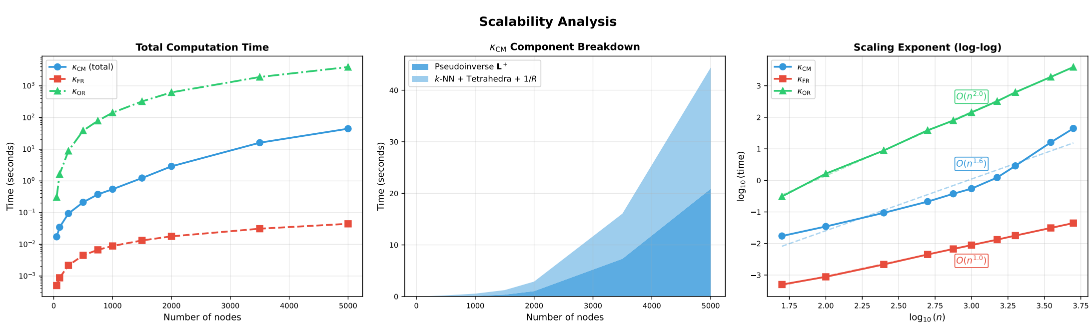

FIG. 3. Computational scalability on Barabási-Albert graphs ($m = 3$) with n from 50 to 5000. **Left:** Total wall-clock time (log scale). κ_{CM} is approximately two orders of magnitude faster than κ_{OR} across all sizes. **Center:** Breakdown of κ_{CM} computation time into the Laplacian pseudoinverse ($O(n^3)$, dark blue) and the k-NN/tetrahedra/circumradius steps ($O(n)$, light blue). **Right:** Log-log scaling with fitted exponents. κ_{FR} scales as $O(n^{1.0})$, κ_{CM} as $O(n^{1.7})$, and κ_{OR} as $O(n^{2.0})$. All benchmarks on a single core of an Apple M-series processor. **Alt-text:** Three-panel scalability plot for κ_{CM}, κ_{FR}, and κ_{OR} on BA graphs (n from 50 to 5000). Left: total runtime (log scale); κ_{CM} is two orders of magnitude faster than κ_{OR}. Centre: κ_{CM} time decomposed into pseudoinverse and tetrahedra steps. Right: log-log scaling with fitted exponents $O(n^{1.0})$, $O(n^{1.7})$, $O(n^{2.0})$ for κ_{FR}, κ_{CM}, κ_{OR} respectively.

8. Discussion

The results presented above establish several findings that we discuss in turn, together with their implications and natural extensions.

κ_{CM} captures genuinely independent geometric information. The low or negative Spearman correlations between κ_{CM} and both κ_{FR} and κ_{OR} (Table 2), contrasted with the consistently high κ_{FR}–κ_{OR} correlation, demonstrate that κ_{CM} is not redundant with existing discrete curvatures. This independence arises from two design choices: the use of effective resistance (rather than hop distance or local edge counts) as the ground metric, and the extraction of curvature from simplex geometry (circumradii) rather than from combinatorial properties or optimal transport. The fact that independence holds across graphs with diverse topologies—from small social networks to scale-free and block-structured models—suggests it is a robust structural property of the metric rather than an artifact of particular graph families. Crucially, this independence implies that κ_{CM} provides a genuinely new axis of information for any downstream task that uses curvature as a feature, as demonstrated by the community detection experiments.

To shed further light on the geometric aspects highlighted by κ_{CM}, we computed its Spearman correlation with three distance-based centrality measures: closeness centrality, betweenness centrality, and degree. Across the benchmark networks, κ_{CM} correlates positively and significantly with all three (closeness: $|\rho| \in [0.54, 0.99]$; betweenness: $|\rho| \in [0.66, 1.00]$; degree: $|\rho| \in [0.66, 0.95]$, all $p < 0.05$ except betweenness in the Florentine Families network). This is geometrically coherent: nodes that are central in the effective-resistance sense tend to be embedded in more compact, densely-connected neighborhoods, yielding higher κ_{CM} values. Crucially, this correlation with centrality does not explain the independence from κ_{FR} and κ_{OR}—both of which are also correlated with degree in most networks—but rather underscores that κ_{CM} captures a genuine geometric signal about local neighborhood compactness that partially overlaps with centrality while remaining orthogonal to the combinatorial (κ_{FR}) and transport-based (κ_{OR}) perspectives.

Geometric coherence across graph families. The monotone ordering of κ_{CM} values from flat graphs (cycle, tree) through intermediate (grid, RGG) to maximally curved (complete graph) is consistent with the expected geometry in every case tested (Table 1). The vertex-transitive graphs (cycle, complete) yield exactly zero variance, confirming that κ_{CM} correctly identifies structural symmetry. This property holds for any deterministic measure on vertex-transitive graphs; the zero-variance result serves here as a consistency check on the pipeline rather than a claim specific to κ_{CM}.. The boundary effects visible in the grid and RGG—where peripheral nodes show lower curvature than interior nodes—are physically meaningful and mirror the behavior of continuous curvature near boundaries. We note that κ_{CM} is strictly positive by construction (as the circumradius is always positive), and therefore measures the *magnitude* of local geometric compactness rather than signed curvature. This is not a deficiency but rather a complementary perspective: while κ_{FR} and κ_{OR} distinguish positive from negative curvature, κ_{CM} quantifies how tightly the local neighborhood is curved regardless of sign, which is precisely what makes it informative in contexts where κ_{FR} and κ_{OR} agree. A natural direction for future work is to establish a formal convergence theorem relating κ_{CM} to classical Riemannian curvature in the continuum limit, analogous to existing results for κ_{OR} [18].

Practical utility beyond community detection. The community detection results (Table 3 and 4) demonstrate that κ_{CM} alone outperforms κ_{FR} and κ_{OR} by an order of magnitude in ARI on SBMs with clear community structure, and that this advantage stems from the sensitivity of effective resistance to community bottlenecks. The intentionally simple clustering method (hierarchical Ward linkage) was chosen to isolate the discriminative power of the curvature features themselves; integration with more sophisticated methods (spectral clustering, graph neural networks) is a promising avenue that could amplify the observed advantage. The honest failure on the fuzzy SBM—where no curvature measure detects communities—reinforces that κ_{CM} does not hallucinate structure where none exists, a desirable property for any geometric descriptor. Beyond community detection, the geometric nature of κ_{CM} suggests potential applications in link prediction, anomaly detection, and characterization of spatial networks where the distinction between metric and topological properties is physically meaningful.

Computational efficiency and scalability. The scalability benchmarks reveal that κ_{CM} is approximately two orders of magnitude faster than κ_{OR} across all tested sizes (Table 6), making it the more practical choice when both geometric depth and computational feasibility are required. The bottleneck is the $O(n^3)$ Laplacian pseudoinverse, which currently limits applicability to graphs with $n \lesssim 10^4$ nodes. However, this is not a fundamental barrier: established techniques from numerical linear algebra—such as Lanczos-based approximations of $\boldsymbol{L}^+$, randomized SVD, or sparse Cholesky factorizations—could reduce the effective complexity and extend κ_{CM} to significantly larger graphs. Such algorithmic improvements are an active area of research in spectral graph theory and represent a natural next step.

Outlook. The present work defines κ_{CM} for unweighted, undirected graphs. Extensions to weighted graphs (via weighted Laplacians), directed networks (via directed resistance distances), and multiplex or temporal graphs are conceptually straightforward and would broaden the applicability of the method. Validation on large-scale empirical networks from diverse domains—biological, infrastructure, communication—would further establish the practical scope of κ_{CM}. Finally, the connection between κ_{CM} and recent resistance-based curvatures proposed by Devriendt and collaborators [6, 7] deserves theoretical investigation: while the algebraic (matrix-inverse) and geometric (simplex-embedding) approaches operate on the same underlying metric, their formal relationship remains to be elucidated.

9. Conclusions

We have introduced the Cayley-Menger curvature κ_{CM}, a discrete curvature measure for graphs grounded in classical distance geometry. The method constructs local tetrahedra for each node using effective resistance distances, computes the Cayley-Menger determinant to embed them in Euclidean space, and extracts the circumradius as a curvature proxy. Validation on graphs with known geometric properties confirms that κ_{CM} orders flat, hyperbolic, and spherical geometries consistently. Comparison with Forman-Ricci and Ollivier-Ricci curvatures across five benchmark networks reveals that κ_{CM} captures geometric information that is statistically independent of both established measures, while the latter two correlate strongly with each other. As a practical demonstration, κ_{CM} alone achieves an order-of-magnitude improvement over κ_{FR} and κ_{OR} in curvature-based community detection on stochastic block models, though absolute ARI values remain moderate and the baseline (Ward linkage) was chosen for simplicity rather than performance; the result demonstrates the discriminative power of the κ_{CM} feature. Computationally, κ_{CM} is approximately two orders of magnitude faster than κ_{OR} and scales to graphs with several thousand nodes.

These results position κ_{CM} as a complementary member of the discrete curvature toolkit, offering a perspective rooted in distance geometry that is distinct from the combinatorial (Forman) and optimal-transport (Ollivier) paradigms. Future directions include the development of convergence theorems linking κ_{CM} to Riemannian curvature, scalable approximation algorithms for the effective resistance computation, and application to empirical networks in domains where geometric structure is physically meaningful, such as spatial networks, brain connectomes, and time series visibility graphs.

Data Availability and Code Availability

All graphs used in this study are either generated programmatically (stochastic block models, Barabási-Albert, grid lattice, balanced tree, cycle, complete graph, random geometric graph) with fixed random seeds for reproducibility, or are publicly available benchmark datasets included in the NetworkX Python library [12, 20, 27]. No external datasets were used.

For the purposes of reproducibility of results and extensions that arise from the code used, the complete Python implementation of the Cayley-Menger curvature (`cm_curvature_pkg`), all analysis scripts, and the LaTeX source of this manuscript are publicly available at https://github.com/sierraporta/Cayley-Menger-Graph-Curvature.

Conflict of Interest

The author declares no competing financial or non-financial interests.

Acknowledgment

The author acknowledges the support of the Universidad Tecnológica de Bolívar (UTB) and the Dirección de Investigaciones y Extensión and the research group of Gravitación y Matemática Aplicada (GIGMA). Computational resources were provided by the author's institutional facilities.

References

1. Alfakih, A. Y. (2018) *Euclidean distance matrices and their applications in rigidity theory*. Springer.

2. Barabási, A.-L. & Albert, R. (1999) Emergence of scaling in random networks. *science*, **286**(5439), 509–512.

3. Blumenthal, L. M. (1972) Theory and Applications of Distance Geometry. *The Mathematical Gazette*, **56**(396), 160.

4. Cayley, A. (1841) On a theorem in the geometry of position. *Cambridge mathematical journal*, **2**, 267–271.

5. Danon, L., Diaz-Guilera, A., Duch, J. & Arenas, A. (2005) Comparing community structure identification. *Journal of statistical mechanics: Theory and experiment*, **2005**(09), P09008–P09008.

6. Devriendt, K. & Lambiotte, R. (2022) Discrete curvature on graphs from the effective resistance. *Journal of Physics: Complexity*, **3**(2), 025008.

7. Devriendt, K., Ottolini, A. & Steinerberger, S. (2024) Graph curvature via resistance distance. *Discrete Applied Mathematics*, **348**, 68–78.

8. Forman, R. (2003) Bochner's method for cell complexes and combinatorial Ricci curvature. *Discrete & Computational Geometry*, **29**(3), 323–374.

9. Hubert, L. & Arabie, P. (1985) Comparing partitions. *Journal of classification*, **2**(1), 193–218.

10. Jost, J. & Liu, S. (2014) Ollivier's Ricci curvature, local clustering and curvature-dimension inequalities on graphs. *Discrete & Computational Geometry*, **51**(2), 300–322.

11. Klein, D. J. & Randić, M. (1993) Resistance distance. *Journal of Mathematical Chemistry*, **12**, 81–95.

12. Knuth, D. E. & Knuth, D. (1993) *The Stanford GraphBase: a platform for combinatorial computing*, volume 1. AcM Press New York, New York.

13. Liberti, L. & Lavor, C. (2017) Euclidean distance geometry. *An Introduction to Distance Geometry*, pages 9–18.

14. Liberti, L., Lavor, C., Maculan, N. & Mucherino, A. (2014) Euclidean distance geometry and applications. *SIAM review*, **56**(1), 3–69.

15. Lin, Y., Lu, L. & Yau, S.-T. (2011) Ricci curvature of graphs. *Tohoku Mathematical Journal, Second Series*, **63**(4), 605–627.

16. Menger, K. (1928) Untersuchungen über allgemeine Metrik. *Mathematische Annalen*, **100**(1), 75–163.

17. Ni, C.-C., Lin, Y.-Y., Luo, F. & Gao, J. (2019) Community detection on networks with Ricci flow. *Scientific reports*, **9**(1), 9984.

18. Ollivier, Y. (2009) Ricci curvature of Markov chains on metric spaces. *Journal of Functional Analysis*, **256**(3), 810–864.

19. Ollivier, Y. (2010) A survey of Ricci curvature for metric spaces and Markov chains. In *Probabilistic approach to geometry*, volume 57 of *Advanced Studies in Pure Mathematics*, pages 343–382. Mathematical Society of Japan.

20. Padgett, J. F. & Ansell, C. K. (1993) Robust Action and the Rise of the Medici, 1400-1434. *American journal of sociology*, **98**(6), 1259–1319.

21. Penrose, M. (2003) *Random Geometric Graphs*. Oxford Studies in Probability. Oxford University Press, Oxford.

22. Samal, A., Sreejith, R., Gu, J., Liu, S., Saucan, E. & Jost, J. (2018) Comparative analysis of two discretizations of Ricci curvature for complex networks. *Scientific reports*, **8**(1), 8650.

23. Sandhu, R., Georgiou, T., Reznik, E., Zhu, L., Kolesov, I., Senbabaoglu, Y. & Tannenbaum, A. (2015) Graph curvature for differentiating cancer networks. *Scientific reports*, **5**(1), 12323.

24. Schoenberg, I. J. (1938) Metric spaces and positive definite functions. *Transactions of the American Mathematical Society*, **44**(3), 522–536.

25. Sreejith, R. P., Mohanraj, K., Jost, J., Saucan, E. & Samal, A. (2016) Forman curvature for complex networks. *Journal of Statistical Mechanics: Theory and Experiment*, **2016**(6), 063206.

26. Steinerberger, S. (2023) Curvature on graphs via equilibrium measures. *Journal of Graph Theory*, **103**(3), 415–436.

27. Zachary, W. W. (1977) An information flow model for conflict and fission in small groups. *Journal of anthropological research*, **33**(4), 452–473.